Genetic dissection of glutamatergic neuron subpopulations and developmental trajectories in the cerebral cortex

Katherine S. Matho[1], Dhananjay Huilgol[1#], William Galbavy[1,4#], Gukhan Kim[1#], Miao He[1#,α], Xu An[1], Jiangteng Lu[1,b], Priscilla Wu[1], Daniela J. Di Bella[2], Ashwin S. Shetty[2], Ramesh Palaniswamy[1], Joshua Hatfield[1], Ricardo Raudales[1,4], Arun Narasimhan[1], Eric Gamache[1], Jesse Levine[1,5], Jason Tucciarone[1,5,c], Partha Mitra[1], Pavel Osten[1], Paola Arlotta[2,3], Z. Josh Huang[1,*]

[1]Cold Spring Harbor Laboratory, Cold Spring Harbor, New York 11724, USA.

[2]Department of Stem Cell and Regenerative Biology, Harvard University, Cambridge, MA 02138, USA.

[3]Stanley Center for Psychiatric Research, Broad Institute of MIT and Harvard, Cambridge, MA 02138, USA.

[4]Program in Neuroscience, Department of Neurobiology and Behavior, Stony Brook University, Stony Brook, NY, 11794, USA.

[5]Program in Neuroscience and Medical Scientist Training Program, Stony Brook University, New York 11790, USA.

[*] corresponding author huangj@cshl.edu

[#] equal contribution authors

Current address:

[α]Institute of Brain Sciences, State Key Laboratory of Medical Neurobiology, Collaborative Innovation Center for Brain Science, Fudan University, Shanghai 200032, China.

[b] Shanghai Jiaotong University Medical School, Shanghai, China.

[c] Department of Psychiatry, Stanford University School of Medicine, Palo Alto, CA, USA.

ABSTRACT

Diverse types of glutamatergic pyramidal neurons (PyNs) mediate the myriad processing streams and output channels of the cerebral cortex, yet all derive from neural progenitors of the embryonic dorsal telencephalon. Here, we establish genetic strategies and tools for dissecting and fate mapping PyN subpopulations based on their developmental and molecular programs. We leverage key transcription factors and effector genes to systematically target the temporal patterning programs in progenitors and differentiation programs in postmitotic neurons. We generated over a dozen of temporally inducible mouse Cre and Flp knock-in driver lines to enable combinatorial targeting of major progenitor types and projection classes. Intersectional converter lines confer viral access to specific subsets defined by developmental origin, marker expression, anatomical location and projection targets. These strategies establish an experimental framework for multi-modal characterization of PyN subpopulations and tracking their developmental trajectories toward elucidating the organization and assembly of cortical processing networks and output channels.

INTRODUCTION

Glutamatergic pyramidal neurons (PyNs) constitute the large majority (~80% in rodent) of nerve cells in the cerebral cortex. In contrast to the short-range projecting GABAergic inhibitory interneurons that form cortical local circuitry, the long-range projecting PyNs mediate the myriad inter-areal processing streams and all of the cortical output channels [1-3]. Traditionally, the vast number of PyNs has been broadly classified into a handful of major classes according to their laminar location or broad axon projection patterns, such as intratelencephalic (IT) and extratelencephalic (ET or corticofugal), which further comprises subcerebral (including pyramidal tract-PT) and cortico-thalamic (CT) PyNs [1,4]. It is increasingly evident that these simple schemes belie the substantial diversity and specificity of PyN organization. Subsets of PyNs appear to form specific local and long-range connectivity, linking discrete cortical microcircuits to separate cortical subnetworks and output channels [1,5]. Recent single cell RNA sequencing analysis suggests over a hundred PyN transcriptomic types from just two cortical areas [6]. As the definition and systematic identification of PyN types require establishing correspondence across molecular, anatomical and physiological properties, reliable experimental access to specific PyN subpopulations is not only necessary for such multi-modal integration but also for exploring their circuit function. However, genetic tools for PyN subpopulations are severely limited, and the experimental strategy for a systematic dissection of PyN subpopulations that reflect their circuit organization has not been established.

Despite their immense number and diversity, all PyNs are generated from neural progenitors seeded in the embryonic dorsal telencephalon. Classic studies have established that a protomap of regionally differentiated radial glial progenitors (RGs) lining the cerebral ventricle undergo repeated rounds of asymmetric divisions and give rise to radial clones of PyNs, which are sequentially deployed to the cortex in a largely inside-out order [7]. RGs generate PyNs either directly or indirectly through intermediate progenitors (IPs), which divide symmetrically to generate pairs of PyNs [8]. Recent scRNAseq analysis at multiple developmental stages have revealed a set of key temporal patterning genes that drive lineage progression in RGs, and a largely conserved differentiation program that unfolds in successively generated postmitotic neurons [9]. Together, these studies delineate an outline of the cellular and molecular logic of PyN development [3,9,10]. However, the diversity and lineage organization of cortical progenitors remain unresolved and debated [11-14], and it is unclear whether different RG subpopulations (e.g. marked by transcription factor expression) and neurogenetic mechanisms (direct vs indirect) contribute, ultimately, to projection-defined PyN subpopulations. Resolving these fundamental issues requires genetic fate mapping tools with sufficient progenitor type resolution and temporal precision that enable tracking the developmental trajectory of PyNs.

Among the challenges of establishing genetic access to PyN types, the first and foremost is specificity (with an appropriate granularity) and the second is comprehensiveness. Although a large number of transgenic driver lines have been generated that label subsets of PyNs, only a handful are specific and reliable enough for neural circuit analysis [15,16]. More importantly, as there is no simple relationship between single gene expression and "neuron types", it is not clear whether and how a systematic dissection of PyN types can be achieved. Here, we have generated and characterized a set of 15 *Cre* and *Flp* gene knockin mouse driver lines for targeting PyN progenitors and subpopulations, guided by

knowledge in their developmental genetic programs. Orthogonal and temporally inducible drivers enable combinatorial targeting of major progenitor types (e.g. TF-defined RGs, IPs, neurogenic progenitors) and projection classes (e.g. CT, PT, IT subclasses and subpopulations within). Intersectional converter lines confer viral access to specific subsets defined by cell birth time, marker expression, anatomical location and projection targets. These tools and strategies establish an experimental framework for accessing hierarchically organized PyN projection types at progressively finer resolution. They will not only facilitate systematic multi-modal analysis of PyN subpopulations to define cortical circuit elements but also enable tracking their developmental trajectories toward elucidating the organization and assembly of processing networks and output channels of the cerebral hemisphere, including the cortex, hippocampus, and basolateral amygdala.

RESULTS

Our overarching strategy is to engage the precise spatiotemporal gene expression patterns of the specification and differentiation programs to target biologically relevant progenitor subsets, PyN subpopulations, and their developmental trajectories (Fig. 1). As such our approach differs from previous efforts [15,16] in several significant ways. First, we use gene knockin (KI) instead of transgenic approach to precisely recapitulate the endogenous pattern of TFs and effector genes with well-characterized roles demonstrated by developmental genetic studies. Second, as temporal patterning of TF expression is an essential and evolutionarily conserved mechanism for generating cell type diversity, we generated mostly inducible *CreER* driver lines to leverage this versatile and efficient strategy. Third, the high reliability of the KI approach allows strategic design of combinatorial schemes across developmental stages. Fourth, intersectional reporter and converter lines integrate multiple developmental genetic properties and further engage anatomic features for viral targeting of highly specific PyN types.

All KI drivers (except as noted) are generated by in-frame insertion of *CreER* or *Flp* coding cassettes before the STOP codon of an endogenous gene, separated by a T2A self-cleaving peptide sequence (Table 1). Recombination patterns in all driver lines appear to recapitulate the spatial, temporal and cellular gene expression patterns of the targeted endogenous loci, where such data are available (Table 2). These driver and reporter lines are deposited to the Jackson Laboratory for wide distribution. For simplicity, all drivers are named as *GeneX-CreER/Flp*, where *T2A* or *IRES* is omitted.

Progenitor type driver lines enable fate mapping of PyN developmental trajectories

The embryonic dorsal telencephalon contains a developmental ground plan whereby sequential transcription programs drive the proliferation and lineage progression of neuroepithelial and progenitor cells to orderly generate all PyNs in the cortex[3,10,17]. Temporally regulated expression of key TF networks gates sequential developmental decisions at the progenitor, postmitotic and postnatal differentiation stages to progressively shape hierarchically organized PyN classes and subpopulations[10,18].

Probing the diversity of RGs

Among over two dozen major TFs implicated in corticogenesis [18], the LIM-homeodomain protein LHX2 and zinc-finger transcription factor FEZF2 are foundational and act at nearly every stage throughout the construction of the neocortex. *Lhx2* plays multiple essential roles from the initial selection of cortical primordium over the hem and antihem [19-21], to the balance of neuroepithelial proliferation over differentiation, the fate restriction of radial glial cells (RGs), the differentiation of upper layer postmitotic PyNs [22], and the timing of gliogenesis [17]. In a similar yet contrasting way, *Fezf2* is expressed from early RGs and subsequently functions as a master regulator for the specification and differentiation of infragranular corticofugal PyNs [23,24]. Importantly, during the period of deep layer neurogenesis, *Lhx2* suppresses *Fezf2* expression in progenitors through direct binding to its distal enhancer elements, thereby regulating the specification of PyN subtype identity [25]. However, the precise fate potential and temporal progression of *Lhx2*$^+$ and *Fezf2*$^+$ RGs (RGs^{Lhx2}, RGs^{Fezf22}) and their relationship to the lineage organization of cortical progenitors in general, are largely unknown. We have generated *Lhx2-CreER, Fezf2-CreER,* and *Fezf2-Flp* driver lines that enable precise fate mapping of these TF-defined RG pools.

Using the *Lhx2-CreER* driver, we carried out a series of short (~24-hrs) pulse-chase experiments at multiple embryonic stages to reveal the status of the progenitors and lineage progression, as well as a set of long pulse-chase experiments from similar embryonic stages to the mature cortex to reveal the pattern of their PyN progeny. At E10.5, a short tamoxifen (TM) pulse-chase in *Lhx2-CreER;Ai14* embryos resulted in dense and near ubiquitous labeling of NEs and RGs in the dorsal pallium at E11.5, with a sharp border at the cortex-hem boundary (Fig. 2e, Extended Data Fig. 1); this pattern precisely recapitulates the endogenous *Lhx2* expression [26,27]. These early RGs showed characteristic radial fibers and end-feet at the ventricle surface; the position of their soma likely reflected the stage of cell cycle progression, including those dividing at the ventricle surface (Fig. 2e, Extended Data Fig. 1a). E12.5→E13.5 pulse-chase revealed prominent medial^{high} to lateral^{low} gradient of RGs^{Lhx2} (Fig. 2g), suggesting significant differentiation of the earlier E10.5 RG pool. E13.5→E14.5 pulse-chase shows similar gradient pattern at lower overall density (Fig. 2i, Extended Data Fig. 1c), with conspicuous cell clones suggesting the high proliferative capacity of *Lhx2*$^+$ RGs at this stage (Fig. 2i, Extended Data Fig. 1c).

Long pulse-chase from E10.5, E12.5 and E14.5 to mature cortex labeled PyN progeny across cortical layers (Fig. 2f, h, j, Extended Data Fig. 1b, d), suggesting that RGs^{Lhx2} are multipotent at these embryonic stages. E14.5 RGs^{Lhx2}-derived PyNs show lower density in L5/6 and higher density in L2-4, suggesting more restricted fate potential (Fig. 2j). During the early postnatal period, when *Lhx2* expression is mostly postmitotic, pulse-chase labeled PyNs across layers that comprise largely the IT class (Extended Data Fig. 1e). From the second postnatal week, pulse-chase mainly labeled astrocytes (Extended Data Fig. 1f). Together, these results indicate that the *Lhx2-CreER* driver precisely recapitulates endogenous expression across developmental stages and provides a highly valuable fate mapping tool for a TF-defined RG pool.

Similar fate mapping experiments using the *Fezf2-CreER* driver yielded a contrasting set of results. At E10.5, short pulse-chase (with the same TM dose as in the *Lhx2-CreER*) labeled only a sparse set of pallial RG progenitors within the neocortex, sharply ending at the cortex-hem boundary (Fig. 2k,

Extended Data Fig. 1g). E12.5→E13.5 pulse-chase labeled a larger set of RGs^{Fezf2} with a similar medial^{high} to lateral^{low} gradient as RGs^{Lhx2} but with notably lower density (Fig. 2m). RGs^{Fezf2} characteristics were similar to RGs^{Lhx2} at the same stage. By E13.5, short pulse-chase labeled few RGs, mostly in the medial region, and the rest were postmitotic PyNs (Fig. 2o, Extended Data Fig. 1i).

Long pulse-chase from E10.5 and E12.5 to P30 cortex in *Fezf2-CreER* mice labeled PyNs distributed across cortical layers, suggesting multi-potent RGs^{Fezf2} between E10.5-E12.5 (Fig. 2l, n; Extended Data Fig. 1h). After E13.5, Fezf2 expression is mostly shifted to postmitotic L5/6 corticofugal PyNs, especially in the lateral cortical primordium (Fig. 2o, p, Fig. 3, Extended Data Fig. 4). Therefore, contrasting a *Fezf2* transgenic line [13], the *Fezf2-CreER* driver also recapitulates endogenous developmental expression and provides a valuable fate mapping tool for the RGs^{Fezf2} pool.

Together, results from the *Lhx2-* and *Fezf2- CreER* drivers revealed partially overlapping as well as possibly distinct RG pools. Although early RGs^{Fezf2} and RGs^{Lhx2} are both multipotent in generating PyNs across layers, their progeny might differ in terms of projection pattern and connectivity when analyzed at cellular and clonal resolution; this can be achieved by converting transient *CreER* activity that captures lineage progression in progenitors to a permanent toolgene expression (e.g. Flp, tTA) in progeny PyNs for viral-based phenotypic characterization and manipulation [28](also see Fig. 5,6).

Probing the diversity of neurogenic RGs (nRGs)

The early cortical progenitors comprise proliferative as well as neurogenic subpopulations, likely with different fate potentials. *Tis21* is an anti-proliferative transcription co-regulator that negatively controls cell cycle checkpoint and is specifically expressed in subsets of RGs that undergo neurogenic but not proliferative cell divisions [29,30]. It is unknown whether the neurogenic RGs (nRGs) at any particular time are homogeneous or consist of subpopulations with differential TF expression and fate potential. We developed a novel fate mapping strategy to address this issue. To target nRGs, we generated a *Tis21-CreER* driver line (Extended Data Fig. 2). As *Tis21* is also expressed in neurogenic progenitors of the ventral subpallium, 48hr pulse-chase from E10.5 revealed prominent nRG-derived clones along both the pallium-glutamatergic and subpallium-GABAergic progenitor domains (Extended Data Fig. 2a). E10→P30 long pulse-chase revealed columnar arrangement of PyN and astrocyte clones, intermixed with subpallium-derived GABAergic interneurons (Extended Data Fig. 2b).

To restrict fate mapping to glutamatergic nRGs and probe their diversity, we designed an intersection/subtraction scheme to differentially label nRGs that either express or do not express *Fezf2*. First, we generated a *Fezf2-Flp* driver, which recapitulated endogenous *Fezf2* expression (Extended Data Fig. 5h-n). We then carried out intersection/subtraction fate mapping using *Tis21-CreER;Fezf2-Flp;IS* mice (Fig. 2t,u, Extended Data Fig. 2c,d). E11.5→E12.5 or E13.5 pulse-chase demonstrated that *Tis21/Fezf2* intersection specifically labeled a set of pallial nRGs with GFP, whereas *Tis21/Fezf2* subtraction labeled subpallial nRGs with RFP (Fig. 2t, Extended Data Fig. 2c). The result further revealed that pallial nRGs consisted of both *Fezf2*$^{+}$ (GFP) and *Fezf2*$^{-}$ (RFP) subpopulations (Fig. 2t; Extended Data Fig. 2c), suggestive of heterogeneity. There was no apparent morphological difference between *Fezf2*$^{+}$ and *Fezf2*$^{-}$ nRGs.

Long pulse-chase from E12→P30 revealed three types of PyN clones. RFP-only clones likely derived from *Fezf2*$^{-}$ nRGs in which *Tis21-CreER* activated RFP expression. They likely consisted of PT cells that did not express *Fezf2* at any stage (Extended Data Fig. 2d,e). The GFP-only clones likely derived from *Fezf2*$^{+}$ nRGs, in which *Tis21-CreER* and *Fezf2-Flp* co-expression activated GFP in the *IS* reporter allele (Extended Data Fig. 2d', f). The mixed GFP-RFP clones are likely derived from *Fezf2*$^{-}$ nRGs in which *Tis21-CreER* first activated RFP expression followed by postmitotic activation of GFP through *Fezf2-Flp* (Fig. 2u, Extended Data Fig. 2d, d', g). Together, these results indicate the presence of *Fezf2*$^{+}$ as well as *Fezf2*$^{-}$ nRGs, both multi-potent in generating PyNs across all cortical layers. It remains to be examined whether their progeny might differ in terms of projection pattern and connectivity when analyzed at cellular and clonal resolution. This intersection/subtraction strategy can be used to fate map the diversity of nRGs with other TF Flp drivers.

Targeting intermediate progenitors

IPs and indirect neurogenesis have evolved largely in the mammalian lineage and have continued to expand substantially in primates [29,31-33]. Along the mammalian embryonic neural tube, indirect neurogenesis is restricted to the telencephalon and is thought to contribute to the expansion of cell numbers and diversity in the forebrain, especially the neocortex. Indeed, the majority of PyNs in mouse cortex are produced through indirect neurogenesis [34-36]. But the temporal patterns of IP-mediated indirect neurogenesis in relation to their PyN progeny are not well characterized. The T-box transcription factor *Tbr2* is specifically expressed in pallial IPs throughout indirect neurogenesis [37,38]. We have generated both *Tbr2- CreER* and *FlpER* driver lines.

Embryonic 12 hr pulse-chase at E16.5 with *Tbr2-CreER* revealed specific labeling of IPs and not RGs (Fig. 2q). Long pulse-chase E16→P30 labeled PyNs in L2/3, which are expected to be generated at this embryonic stage (Fig. 2r, Fig. 3b). In addition, fate mapping of *Tbr2-CreER;Ai14* from E17 to P28 revealed highly laminar restricted PyN cohorts in L2 (Fig. 3b). Therefore the *Tbr2- CreER* driver can achieve highly specific targeting of PyN laminar subpopulations in supragranular layers.

Whereas most IPs undergo a single symmetric division to produce two PyNs, a subset are transit amplifiers, each first generate two IPs which then divide to produce a total of 4 PyNs[39]. To specifically target neurogenic IPs that also express *Tis21*, we combined *Tis21-CreER* and *Tbr2-FlpER* with the intersectional reporter Ai65. E16→P30 fate mapping resulted in similar laminar pattern of PyN progeny as using *Tbr2-creER* and Ai14, consistent with the notion that most *Tbr2*$^{+}$ IPs in the mouse dorsal pallium are neurogenic instead of transit-amplifying (Fig. 2s). The *Tbr2-CreER* and *FlpER* driver lines thus allow efficient fate mapping and manipulation of pallial IPs.

Altogether, these progenitor driver lines enable specific and temporally controlled targeting of major pallial progenitor types (RGs, nRGs, IPs) and TF-defined subpopulations for exploring the diversity of progenitors and their lineage progression. They will facilitate tracking the developmental trajectories of PyNs from their lineage origin to postmitotic differentiation, migration, laminar deployment, circuit assembly and function.

Driver lines targeting projection subpopulations

A useful genetic toolkit for PyNs would comprise driver lines that target their hierarchical organization[6], including major projection classes and finer biologically meaningful subpopulations within each class. Previous efforts have produced approximately a dozen mostly transgenic lines targeting several major laminar and projection subpopulations [15,16]. Complementary to this effort, we designed gene KI drivers based on key TFs and effector genes of the molecular and developmental programs of PyNs to access more and biologically relevant subpopulations toward dissecting cortical circuit elements [10,18,40-42] (Fig. 3a). These inducible drivers further confer temporal control at different developmental stages and TM dose-dependent labeling and manipulation from sparse individual cells to dense populations.

IT driver lines

The intratelencephalic (IT) PyNs constitute the largest top-level class and mediate the vast majority of intracortical, inter-hemispheric, and cortico-striatal communication streams [1,43-45]. Currently, several IT-directed driver lines are available (Fig. 3a), including the *Cux2-CreER* [11] and *Rasgrf2-dCre* [16] KI lines and the *Tlx3-Cre* transgenic line [15].

Cux1 and *Cux2* are Cut-repeat containing homeodomain TFs predominantly expressed in supragranular IT PyNs and their progenitors [46,47]. *Cux* gene expression is thought to begin at the transition from progenitor to postmitotic neurons [46,48], thus may initiate and then maintain the stable identity of IT PyNs. Although *Cux1* and *Cux2* exhibit similar DNA binding specificities and most upper layer neurons co-express the two proteins, they appear to play non-redundant and additive roles in coordinating the progression of cell fate programs and in regulating dendritic branching and synapse stabilization [49]. In particular, *Cux1* but not *Cux2* promotes the development of contralateral axonal connectivity of L2/3 IT cells by regulating their firing mode [50]. We generated a *Cux1-CreER* driver. TM induction at P21 in *Cux1-CreER;Ai14* mice labeled prominently L2-4 PyNs largely dorsal to the rhinal fissure, recapitulating the endogenous pattern (Fig. 3b). *Cux1-CreER* thus provides reliable access to supragranular PyNs in the cortex and a set of hippocampal PyNs.

The plexinD1-semaphorin3E receptor-ligand system has been implicated in neuronal migration, axon guidance, synapse specification [36,51], as well as vascular development [52]. In developing and mature cortex, *PlxnD1* is expressed in large sets of callosal projection IT PyNs (CPNs) at especially high levels during early the postnatal period of synapse maturation and refinement [42,53]. We generated *PlxnD1-CreER* and *PlxnD1-Flp* lines. Both drivers recapitulated endogenous PlxnD1 expression and labeled projection neurons in the cerebral cortex, hippocampus, amygdala (BLA and LA), and medium spiny neurons of the striatum (Fig. 3b, 6e, Extended Data Figure 3, Table 2, Supplementary Mov.1&2). In neocortex, L5A and L2/3 IT PyNs were labeled, with their axons predominantly restricted to the cortex and striatum (Fig. 3b). In the piriform cortex L2 PyNs were targeted in both *PlxnD1-CreER* and *PlxnD1-Flp* lines. As PlxnD1 is also expressed in a set of vascular cells (Extended Data Fig. 6), we bred *PlxnD1-CreER* with the neuron-specific reporter *Snap25-LSL-GFP* to achieve selective labeling of *PlxnD1*$^{+}$PyNs (PyNs^{PlxnD1} Fig. 3b).

Cell type specific anterograde tracing using our CreER→Flp conversion strategy (Fig. 4a) and Flp-activated AAV-fDIO-GFP from whisker somatosensory barrel cortex (SSp) reveals that PyNs^{PlxnD1}

project to ipsi- and contra-lateral cortical and striatal regions (Fig. 4, Extended Data Fig. 5a, b, o-t, Supplementary Table 3, Supplementary Movie 3). Together, the *PlxnD1-CreER* and *PlxnD1-Flp* drivers provide versatile experimental access to this major IT subpopulation and to the *PlxnD1*$^{+}$subpopulations in the striatum and amygdala.

The supragranular layers comprise diverse IT neurons that project to a large combination of ipsi- and contra-lateral cortical and striatal regions [41,45,53], but only a few L2/3 driver lines have been reported to date [16], and none distinguish L2 vs L3 PyNs. We used a different approach to target L2/3 PyNs by engaging cell lineage and birth timing. In our *Tbr2-CreER* driver targeting intermediate progenitors (Figure 2q), tamoxifen induction at E16.5 and E17.5 specifically labeled PyNs L2/3 and L2, respectively (Fig.3b). Combined with the CreER→Flp conversion strategy that converts transient lineage and birth timing signals to permanent Flp expression [28], this approach enables specific AAV manipulation of L2 and L3 IT neurons.

PT drivers

Following its early expression in a subset of dorsal pallial progenitors, *Fezf2* becomes restricted to postmitotic L5 and L6 corticofugal PyNs, with high levels in L5B PT and low levels in a subset of CT neurons [42,54]. At postnatal stages, *Fezf2-CreER* and *Fezf2-Flp* drivers precisely recapitulate endogenous postmitotic *Fezf2* expression (Fig. 3c, Extended Data Fig. 3, 4, 5). *Fezf2-CreER;Ai14* labeled projection neurons in the cerebral cortex, hippocampus, amygdala, olfactory bulb and sparsely in the cerebral nuclei (striatum, nucleus accumbens and olfactory tubercle) (Table 2, Supplementary Movie 4). Within the neocortex, PyNs^{Fezf2} are predominantly located in L5B and to a lesser extent in L6 (Fig. 3c, Extended Data Fig. 3a, 4a). There was a conspicuous lack of expression in the evolutionarily more ancient cortical regions below the rhinal fissure. Retrograde labeling with fluorogold tracer from cervical spinal cord in a Fezf2;Ai14 mouse reveals that ~95% spinal cord-projecting PT neurons are Fezf2+. Anterograde mapping of PyNs^{Fezf2} in SSp revealed axon projections to numerous somatomotor cortical (e.g. ipsilateral vibrissal MOs) and subcortical regions including striatum, VPM and POm in the thalamus, anteropretectal nucleus, superior colliculus, pontine nucleus and spinal trigeminal nucleus (Fig.4, Extended Data Fig. 5a, b, h-n, Supplementary Table 3, Movie 5).

In addition to the *Fezf2* drivers targeting the broad corticofugal class, we further generated several lines targeting subpopulations. *Adcyap1* encodes a neuropeptide and is a transcriptional target of *Fezf2* [55], expressed in a subset of PyNs^{Fezf2} located in upper L5B mainly during the postmitotic and perinatal stage. Late embryonic TM induction in *Adcyap1-CreER* recapitulated endogenous expression pattern (Fig. 3c, Extended Data Fig. 3, 4, Supplementary Movie 6). Anterograde tracing of PyNs^{Adcyap1} revealed overlap with PyNs^{Fezf2} (Fig. 4, Extended Data Fig. 5a, b, Supplementary Table 3, Movie 7).

Tcerg1l is a transcription elongation regulator expressed in a subset of L5 corticofugal PyNs during postmitotic and early postnatal stages [42]. TM induction at P21 in *Tcerg1l-CreER* labels a subset of L5B PyNs (Fig. 3c, Extended Data Fig. 3, 4, Supplementary Movie 7). It is currently unclear how these PyNs^{Tcerg1l} relate to PyNs^{Fezf2}. Anterograde AAV labeling of PyNs^{Tcerg1l} revealed overlap with PyNs^{Fezf2} but absence of the collateral to first-order thalamic nucleus VPM (Fig. 4, Extended Data Fig. 5a, b, Supplementary Table 3, Movie 8).

SEMA3e engages in ligand/receptor interactions with PLXND1 to regulate axon guidance and synapse specificity [52]. *Sema3e* is expressed in a subset of L5B PyNs primarily in the sensory areas [56,57]. The *Sema3e-CreER* driver [58] labels a subset of L5B PyNs (Fig. 3c; Extended Data Fig. 3; Supplementary Movie 9). Anterograde AAV labeling reveals that PyNs^{Sema3E} project to more restricted subcortical areas, namely higher order thalamic nucleus POm and pontine nucleus (Extended Data Fig. 5c-g). Together, this new set of driver lines facilitates experimental access to a set of genetically-defined PT PyNs.

CT driver lines

The T-box transcription factor *Tbr1* is thought to represent an obligatory step of the TF cascade of PyN neurogenesis and was thought to express in most if not all newly postmitotic PyNs [59]. Tbr1 then becomes mainly restricted to L6 CT neurons and directly represses the expression of Fezf2 and Ctip2 to suppress the SCPN (PT) fate [10,60]. TM induction at P4 in our *Tbr1-CreER* driver labeled dense L6 CT neurons, with sparse labeling in L2/3, as well as subsets of cells in OB, cerebral nuclei (i.e. pallidum), hippocampus (i.e. dentate gyrus), piriform cortex, and sparse expression in amygdala (Figure 3d; Table 2; Supplementary Movie 9).

Transducin-Like Enhancer Of Split 4 (*Tle4*) is a transcription corepressor expressed in a subset of CT PyNs [42,61]. Our *Tle4-CreER* driver specifically labels L6 CT PyNs across the cortex, which may consist of two subpopulations with apical dendrites in L4/5 and L1, respectively (Fig. 3d, Extended Data Fig. 3, 4, Supplementary Movie 11). Tle4 is also expressed in medium spiny neurons of the striatum, OB, hypothalamus, superior colliculus, cerebellum, septum and sparsely in the hippocampus, amygdala and brainstem (Table 2, Supplementary Movie 10). Anterograde tracing reveals that PyNs^{Tle4} in SSp project specifically to first order thalamic nucleus VPM (Fig. 4; Extended Data Fig. 5a,b,h-n; Supplementary Table 3). Retrograde labeling confirms two subpopulations of Tle4 CT subtypes based on L4 and L1 dendrites (Extended Data Fig. 6f).

The forkhead/winged helix transcription factor *Foxp2* is thought to be expressed in many CT neurons from postmitotic stage to mature cortex, and transiently expressed by a minor subset of PT neurons in the first postnatal week [62,63]. We characterized a *Foxp2-IRES-Cre* KI line [64] by systemic injection of Cre dependent AAV9-DIO-GFP in 2 month old mice to reveal its brain-wide cell distribution pattern. Cortical labeling was restricted to L6 PyNs, and *Foxp2*$^{+}$ cells were found in multiple other brain regions, including striatum, thalamus, hypothalamus, midbrain (periaqueductal gray, superior and inferior colliculi), cerebellum and inferior olive (Fig. 3d, Table 2, Supplementary Movie 12). Injection of Cre-dependent AAV8-DIO-GFP to SSp barrel cortex revealed the PyN^{Foxp2} axon projection to thalamus, tectum and some ipsilateral cortical areas (Fig. 4; Supplementary Table 3; Supplementary Movie 13). Compared to PyNs^{Tle4}, PyN^{Foxp2} projected more broadly to thalamus, overlapping with the PyN^{Fezf2} projection to thalamus.

To further validate and characterize several PyN driver lines, we carried out a set of histochemical analysis using a panel of class-defining markers (Extended Data Fig. 4). The laminar pattern and class-specific marker expression in *Fezf2-, Tcerg1l-, Adcyap1-, Tle4-* driver lines precisely recapitulated endogenous patterns, demonstrating the reliability and specificity of these lines.

Furthermore, by combining a CreER and a Flp allele into the same mouse, we were able to differentially target PyNs^{Fezf2} and PyNs^{Tle4} (Extended Data Fig. 5h-n) or PyNs^{Fezf2} and PyNs^{PlxnD1} (Extended Data Fig. 5o-t) in the same mouse.

Combinatorial genetic and retrograde viral targeting of projection types

Our anterograde tracing results demonstrate that most marker-defined PyN subpopulations project to multiple brain regions (Fig. 4). To examine whether each subpopulation may comprise multiple projection types with more restricted targets and laminar location, we used retrograde AAV (retroAAV2) to trace from a defined target in a few driver lines (Fig. 5, Extended Data Fig. 6).

First, we used an intersection/subtraction (IS) method to reveal PyNs jointly defined by a marker and a projection target. We bred the *Fezf2-CreER* driver with an IS reporter [28]. In *Fezf2-CreER;IS* mice, *Cre* recombination labels the broad PyNs^{Fezf2} with RFP, while injection of retroAAV2-Flp causes GFP expression in the subset of PyNs^{Fezf2} projecting to the injection target (Fig. 5a, b). Indeed, retroAAV2-Flp injections revealed that PyNs^{Fezf2} with branches to the striatum were located in top L5, those with collaterals to POm thalamus or superior colliculus were restricted to middle and lower portion of L5B, and those projecting to the contralateral spinal trigeminal nucleus (Sp5) in the brainstem were located in the lower portion of L5B (Fig. 5c, d). Using a similar approach in *PlxnD1-CreER;IS* mice, retroAAV2 -*FLEX-tdTomato* labeling from the striatum revealed that while L5A PyNs^{PlxnD1} projected to both ipsi- and contra-lateral striatum, L2/3 PyNs^{PlxnD1} projected mostly to the ipsilateral striatum (Extended Data Fig 6g-l). Furthermore, in the *Tle4-CreER;IS* mice, retrograde tracing from the VPM thalamus revealed two subpopulations of L6 PyNs^{Tle4}, one extended apical dendrites to L4/5 border while the other to L1 (Extended Data Fig 6f), suggesting differential input to these two subpopulations.

Second, we used a novel strategy (triple trigger) to target PyNs jointly defined by a marker (driver line), a projection target, and a cortical location. We generated a new intersectional reporter, *dual-tTA*, that converts Cre and Flp expression to tTA expression for AAV manipulation (Fig. 5e). In a compound *Fezf2-CreER;dual-tTA* mouse, retroAAV2-*Flp* injection in the superior colliculus or contralateral Sp5 activated tTA expression in SC- or Sp5-projecting PyNs^{Fezf2} in the cortex, and AAV-TRE-mRuby to SSp barrel cortex then labeled these restricted projection types (Figure 5f). As a control, we injected *AAV-TRE-mRuby* to SSp barrel cortex without retroAAV2-Flp, ensuring that *dual-tTA* expression was dependent on both Cre and Flp (Extended Data Fig 6m).

Using an orthogonal approach to further reveal the diversity of L5B PyNs^{Fezf2}, we compared those that either express or do not express the calcium binding protein parvalbumin. Using the *Fezf2-CreER;Pv-Flp;IS* compound allele mice, we differentially labeled Fezf2^{+}/PV^{-} (RFP) and Fezf2^{+}/PV^{+} (EGFP) PyNs and compared their intrinsic properties using patch clamp recordings in cortical brain slices (Fig. 5g, h). We found that, compared to PV^{-} PyNs^{Fezf2}, PV^{+} PyNs^{Fezf2} have more depolarized rest membrane potentials and a larger hyperpolarization-activated depolarization. This result suggests that PV^{+} PyNs^{Fezf2} are more excitable and play a stronger rebound activity after the inhibition (Fig. 5h). Whether PV^{-} PyNs^{Fezf2} and PV^{+}PyNs^{Fezf2} have distinct subcortical projection targets remains to be determined.

Combinatorial targeting of PyN subtypes by lineage, cell birth order, marker and anatomy

Compared with the PT and CT classes which are restricted to infragranular layers and generated during the early phase of cortical neurogenesis, IT is a particularly diverse class comprising PyNs across layers that are generated throughout cortical neurogenesis, likely with numerous combinatorial projection patterns to many dozens of cortical and striatal targets. For example, the PyN^{PlxnD1} population as a whole localizes to L5A, L3 and L2 and projects to many ipsilateral and contralateral cortical and striatal targets (Fig. 3b, 4, 6, Extended Data Fig. 5). It is unknown whether PyNs^{PlxnD1} comprise subtypes with more specific laminar and projection patterns. We developed a novel combinatorial method to target PyN ^{PlxnD1} subtypes based on their birth order and anatomy (Fig. 6a). This method is based on the developmental principle that PyN birth time correlates with their laminar position, and the observation that the large majority of IT PyNs are generated from indirect neurogenesis through intermediate progenitors [36].

We generated *PlxnD1-Flp;Tbr2-CreER;Ai65* compound mice by breeding the three alleles. In these mice, the constitutive *PlxnD1-Flp* allele marks the whole population and the inducible *Tbr2-CreER* allele can be used for cell birth dating (Fig 6a). Strikingly, TM induction at E13.5, 15.5 and 17.5 selectively labeled L5A, L3, and L2 PyNs ^{PlxnD1} (Fig. 6b-d). To reveal the projection pattern of these birth-dated PyNs, we bred the *PlxnD1-Flp;Tbr2-CreER;dual-tTA* compound allele mice. AAV-TRE3g-mRuby injection of SSp barrel cortex in E13.5- and 17.5- induced mice labeled distinct subtypes of PyNs^{PlxnD1} which differ in projection targets. Although they both project to ipsi- and contralateral cortex and striatum, E13.5-born PyNs$^{PlxnD1(E13.5)}$ resided in L5A and project strongly to contralateral temporal association area (TEa) and striatum, as well as to contralateral cortex and striatum, while E17.5-born PyNs$^{PlxnD1(E17.5)}$ resided in L2, with minimum projection to contralateral TEa and striatum and a strong projection to homotypic contralateral cortex (Fig. 6g-u). Importantly, these two PyNs^{PlxnD1} further differed in terms of their axon termination pattern within the cortical target area. Whereas PyNs$^{PlxnD1(E13.5)}$ axons terminated in the full thickness of L1 and L2/3, with few axon branches in L5A, PyNs$^{PlxnD1(E17.5)}$ axons terminated strongly in L2/3 and L5A, with weak or few axons in L1 (Fig. 6l, m, s, t, u). This result reveals that, even within the same target areas, PyNs$^{PlxnD1(E13.5)}$ and PyNs$^{PlxnD1(E17.5)}$ may preferentially select different postsynaptic elements (e.g. cell types and/or subcellular compartments). The tight correlation between cell birth time, laminar location, projection target, and axon termination pattern suggests that the diversity of PyNs^{PlxnD1} is unlikely to arise from stochastic processes but rather from the developmental program. This approach also demonstrates that it is feasible to target highly specific PyN subtypes by a strategic combination of developmental (lineage, birth order), molecular and anatomical attributes using just three alleles and one viral vector. The same approach can be combined with retrograde tracing approaches to further target PyNs subtypes based on specific projection targets.

DISCUSSION

Specific and systematic experimental access to PyN subpopulations is prerequisite to deciphering the hierarchical organization and developmental assembly of cortical circuit elements by integrating molecular, anatomical and physiological properties as well as their developmental trajectories [2]. Here, we present genetic tools and strategies for dissecting PyN subpopulations and tracking their

developmental trajectories. Together with previous resources [15,16,65], these driver lines provide substantial coverage of major PyN classes and subpopulations (Fig. 3a). The multiple inducible driver lines targeting several progenitor types and subpopulations provide essential tools for fate mapping studies to explore the developmental logic and mechanisms of PyN specification, differentiation, and circuit assembly. The combinatorial method that engages lineage, birth order, marker genes, and anatomy allows highly specific targeting of PyN subtypes with 2-3 driver/reporter alleles. These strategies and tools establish an experimental framework for accessing PyN subpopulations and tracking their developmental trajectories.

The relationship between current and previously reported driver lines targeting similar PyN classes remains to be further characterized at the cellular resolution. A fundamental difference between the transgenic and gene KI approach to cell type targeting is the "nature" of regulatory mechanisms that drive tool-gene (e.g. CreER, Flp) expression. Transgene expression results from the ectopic interactions of the transgenic promoter/enhancers with the surrounding gene regulatory elements at a random genomic integration site [66], giving rise to an arbitrary spatial and temporal "composite expression pattern" that often comprises an artificial mixture of cells. Desirable transgenic expression patterns are identified through screening multiple lines in which the same transgene is integrated at different genomic loci. Although very useful once characterized, each transgenic expression pattern is unique (i.e. integration site dependent) and is not readily reproducible for designing intersection/subtraction patterns to target more restricted subpopulations. In contrast, the vast majority of KI lines precisely recapitulate the endogenous spatiotemporal and cellular gene expression patterns that reflect endogenous developmental processes, physiological mechanisms, and tissue organization. Thus, the usefulness and impact of KI lines depend on the choice of targeted genes based on prior knowledge. Our effort has focused on key transcription factors and effector genes implicated in the specification, differentiation, and maintenance of PyN cell fate and phenotypes [3,10,18]. These KI driver lines thus enable investigators to parse biologically relevant PyN subpopulations through their inherent developmental, anatomical and physiological properties, i.e. "carving nature at its joints". This scheme enables further combinatorial targeting of finer projection types through marker intersections and viral tools that incorporate anatomy and projection properties.

As most endogenous and trans-genes that show restricted expression to PyN subpopulations are often more broadly expressed at earlier developmental stages, many constitutive Cre lines are often not suited to take advantage of the highly valuable tool-gene reporter lines [65] because Cre recombination patterns integrate across time and become non-specific to the intended PyN subpopulation in mature cortex. The temporal control of our inducible driver lines confers major advantages of specificity and flexibility in cell targeting, functional manipulation, and developmental fate mapping toward exploring circuit organization and assembly. Inducibility also allows investigators to control the density of labeling and manipulation of PyN subpopulations, from dense coverage to single cell analysis. Importantly, single cell analysis provides the ultimate resolution to examine the variability and/or reliability of individual neurons within driver and anatomy defined PyN subpopulations [67], and can be better achieved by inducible driver lines [68] . Furthermore, temporal control allows gene manipulations (e.g. using conditional alleles) in specific subpopulations at different developmental stage to discover the cellular and molecular mechanisms of circuit development and function.

Several of the TFs may represent terminal selector genes involved in both the specification and maintenance of PyN cardinal identity [69] (e.g. Fezf2 for PT neurons and Lhx2, Cux1/2 for IT neurons). Thus, beyond experimental access to PyN subpopulations in mature cortex, the inducible TF driver lines represent powerful "functional fate mapping" tools for tracking the developmental trajectory of PyN types, from their specification to migration, differentiation, connectivity and to circuit function. Importantly, the expression and function of these TFs continue to evolve across mammalian species from rodents to primates and human [70]; they might contribute to the development of human specific traits. For example, *Cux1* is located in the human accelerated region (HAR) of the human genome [71]; and the regulation of Cux1, Fezf2, Tbr1, Tbr2, and Foxp2 continues to evolve and diverge in primates and are implicated in several developmental disorders such as autism [47,59,62]. Therefore, these TF mouse driver lines may provide crucial handles to track the developmental trajectories of PyN subpopulations in the convoluted process of cortical circuit assembly, with implications in the evolutionary history of PyNs in human cortex. This will facilitate deciphering the genetic architecture of developmental disorders by linking gene mutations (e.g. with conditional alleles) to their impact on the developmental trajectory of specific neuron types and altered cortical circuit wiring and function.

Single cell transcriptomic analyses have identified dozens of marker gene combinations that define transcriptomic types [6]. Our study suggests that strategic design of intersectional scheme, leveraging established and characterized driver lines, will substantially expand and improve the specificity and comprehensiveness of PyN targeting. Recent advances in enhancer-based usage of AAV vectors show significant promise in achieving subpopulation restriction [72]. The intersection of enhancer AAVs with strategically designed driver lines may substantially increase the specificity, ease, and throughput of neuronal cell type access.

METHODS

Generation of New Knockin Mouse Lines

Driver and reporter mouse lines listed in Table 1 were generated using a PCR-based cloning, as described before and in the Additional Methods[1-3]. All experimental procedures were approved by the Institutional Animal Care and Use Committee (IACUC) of CSHL in accordance with NIH guidelines. Mouse knockin driver lines are deposited at Jackson Laboratory for wide distribution.

Immunohistochemistry

Embryonic tissue was processed as described in the Additional Methods.

Mice were anesthetized (using Avertin) and intracardially perfused with saline followed by 4% paraformaldehyde (PFA) in 0.1 M PB. Following overnight post-fixation at 4°C, brains were rinsed three times and sectioned 50-75 µm thick with a Leica 1000s vibratome. Coronal brain sections stained and imaged as described in the Additional Methods.

Viral Injection and Analysis

Adult mice were anesthetized by inhalation of 2% isofluorane delivered with a constant air flow (0.4 L•min^{-1}) and stereotactic injections were performed as described in the Additional Methods.

Patch clamp recording in brain slice

Neurons in coronal slices (300 μm) containing the somatomotor cortex from >P30 mice were recorded, as described in the Additional Methods.

Serial Two Photon Tomography

Perfused and post-fixed brains from adult mice were embedded in oxidized agarose and imaged with TissueCyte 1000 (Tissuevision) as described [4,5]. For more information, please refer to the Additional Methods in Supplementary Material.

DATA AVAILABILITY

Raw and stitched whole-brain STP imaging data is available from the BICCN Brain Image Library (BIL) (http://www.brainimagelibrary.org/download.html) at the Pittsburgh Supercomputing Center. Anterograde projection datasets can be visualized on the Mouse Brain architecture website (http://brainarchitecture.org/cell-type/projection) with prefix MouseBrain_HUA_U19.

ACKNOWLEDGMENTS

We are grateful to Dr. Richard Palmiter for providing the *FoxP2-IRES-Cre* mouse line and to Dr. Yutaka Yoshida for providing the *Sema3E-CreER* mouse line. We thank Dr. Leyi Li at CSHL for help with generation of knock-in mice, Dr. Sean M. Kelly for contribution to generating and characterizing the *Tis21-2A-CreER* mouse line, Dr. Yongsoo Kim for providing the digital flatmap of the mouse cortex, Dr. Francesco Boato for help in mouse breeding and brain tissue preparation, Dr. Kathleen Kelly for project management. We thank CSHL Laboratory Animal Resources for mouse husbandry. This work was supported in part by the NIH grants 5R01MH101268-05 and 5U19MH114821-03 to Z.J.H. and P.A., 1S10OD021759-01 to Z.J.H., the CSHL Robertson Neuroscience Fund to Z.J.H. P.O. is supported by NIH U01 MH114824-01. D.H. was supported by Human Frontier Science Program long term fellowship LT000075/2014-L and NARSAD Young Investigator grant #26327. R.R. was supported by NRSA F31 Predoctoral Fellowship 5F31MH114529-03. J.T. and J.M.L. were supported by NRSA F30 Medical Scientist Predoctoral Fellowships 5F30MH097425-03 and 5F30MH108333.

AUTHOR CONTRIBUTIONS

Z.J.H and P.A. conceived the study and obtained funding. Z.J.H. coordinated the study.
Z.J.H., P.A., K.M., D.H. designed the experiments. M.H., P.W and E.G. designed and generated all new knock-in mouse lines. K.M., X.A., D.H., R.P., J.H., D.D., J.T., J.M.L., R.R., W.G., E.G., P.W and M.H. conducted mouse breeding, anatomy, immunohistochemistry, imaging, and quantification.
K.M., W.G., X.A., G.K., J.H. and R.P. conducted virus injection experiments.
J.L. performed the patch clamp recording in brain slice. K.M., J.H., R.P., X.A., A.N., P.M. and P.O. performed whole-brain Serial Two-Photon Tomography and analysis of cell distribution and axon projection patterns. Z.J.H. wrote the manuscript with contributions and edits from P.A., K.M., D.H., W.G., M.H., J.L., X.A.

COMPETING INTERESTS

The authors declare no competing interests.

SUPPLEMENTARY INFORMATION is available for this paper.

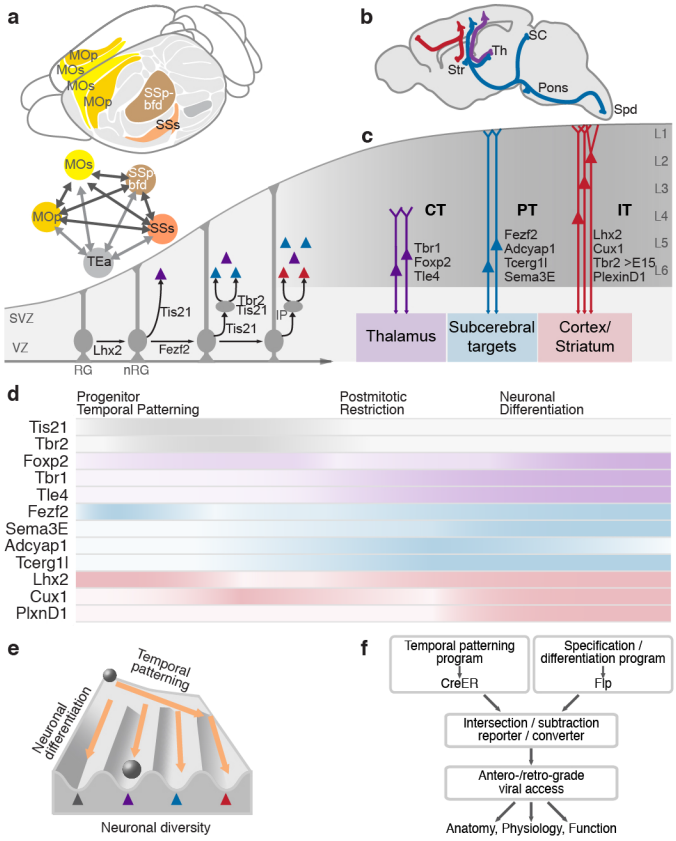

Fig.1 Strategies and tools for targeting PyN subpopulations and developmental trajectories. a, The mouse neocortex consists of multiple cortical areas (upper) that are preferentially interconnected into functional subnetworks, exemplified by the colored sensorimotor network (lower) comprising the primary and secondary sensory (S1-bfd, S2) and motor (M1, M2) cortex and temporal association cortex (TEa). **b,** A schematic sagittal brain section depicting several major PyN projection classes that mediate intra-telencephalic streams (IT-red; cortical and striatal) and cortical output channels (PT-blue, CT-purple). Str, striatum; Th, thalamus; SC, superior colliculus; Spd, spinal cord. **c,** A schematic developmental trajectory of PyNs. During lineage progression, RGs undergo direct neurogenesis and/or indirect neurogenesis through IPs to produce all the laminar and projection types. Genes that are used to target progenitor types and PyN subpopulations are listed according to their cellular expression patterns. VZ, ventricular zone; SVZ, subventricular zone. **d,** Temporal expression patterns of genes used for generating driver lines across major stages of PyN development. Colors correspond to projection classes in **b**; intensity gradients represent approximate changes of expression levels across development for each gene. **e,** The specification and differentiation of PyNs along two cardinal axes: a temporal patterning program in dividing RGs that seeds the successive ground states of their progeny and a largely conserved differentiation program in sequentially born postmitotic PyNs that unfolds the diverse identities. (modified with permission [9]). **f,** A strategy for combinatorial targeting of specific PyN projection types defined by developmental origin, marker expression, anatomical location and projection targets. This is achieved by converting the intersection of two gene expression patterns through *Cre* and *Flp* drivers into viral access that further engage anatomical properties.

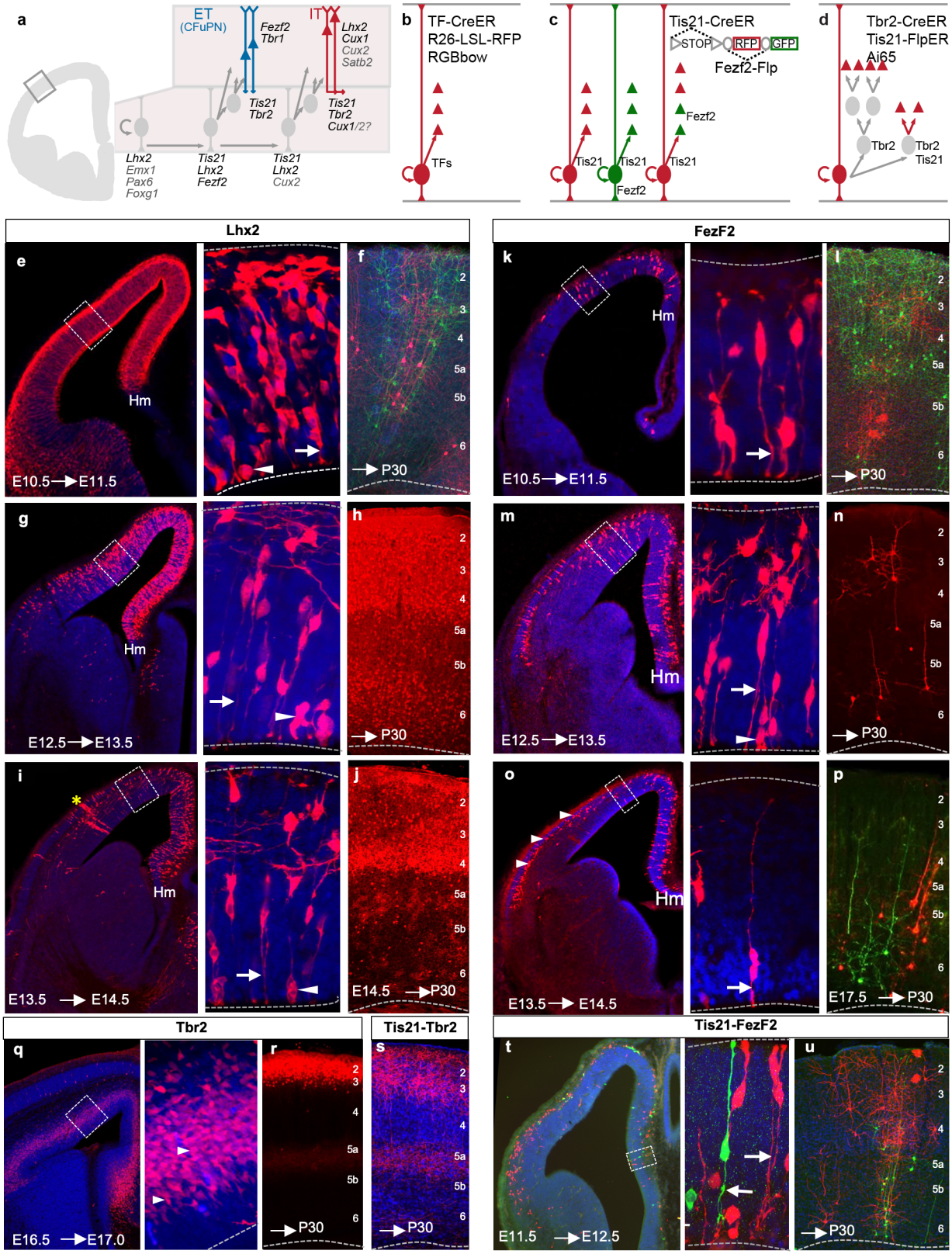

Fig. 2 Driver lines for dissecting progenitor pools and fate mapping PyN developmental trajectories. a, Schematic of the lineage progression of neural progenitors of the embryonic dorsal telencephalon in a hemi-coronal section. Through successive cell divisions, RGs undergo either direct or indirect neurogenesis (through IPs) and give rise to PyNs in different cortical layers and of different projection classes. TFs with key roles in PyN development are listed according to their expression pattern in progenitors (grey) and postmitotic neurons (red and blue); TFs used for generating driver lines are in black. **b,** Fate mapping strategy showing that a specific *TF-CreER* driver labels a RG and all of its progeny with a fluorescent marker when combined with a *Ai14* or a multi-color *RGBow* reporter. This scheme is used in **e-p. c**, Simultaneous fate mapping of different molecularly defined RGs using an intersection/subtraction reporter (*IS*) combined with *Tis21-CreER* and *Fezf2-Flp* drivers. This scheme is used in **t-u.** In *Tis21*$^{+}$*Fezf2*$^{-}$ RGs, Cre activates RFP expression only. In *Tis21*$^{+}$*Fezf2*$^{+}$ RGs, Cre and Flp recombinations remove the RFP cassette and activate GFP expression. At a later stage when *Fezf2* is only expressed in postmitotic deep layer PyNs, *Tis21-CreER* in RGs activates RFP expression in all of its progeny, but RFP is then switched to GFP only in *Fezf*$^{+}$ PyNs expressing Flp. **d**, Fate mapping strategy for IPs and indirect neurogenesis, used in **q-s.** The intersection of *Tis21-CreER* and *Tbr2-FlpER* specifically targets neurogenic IPs but not transit-amplifying IPs when combined with the Ai65 intersectional reporter. **e**, 24-hour pulse-chase in a E10.5 *Lhx2-CreER;Ai14* embryo densely labeled RGs throughout the dorsal neuroepithelium. The magnified view from boxed area shows RGs at different stages of the cell cycle, with endfeet (arrow) or dividing somata (arrowhead) at the ventricle wall (dashed lines). **f**, E10.5 RGs generate PyNs across layers in P28 neocortex using a strategy depicted in **b** with a *Lhx2-CreER;RGBow* mouse. **g**, Same experiment as in **e** except done at E12.5. *Lhx2*$^{+}$ RGs distribute in a medial^{high}-lateral^{low} gradient along the dorsal neuroepithelium, ending sharply at the cortex-hem boundary (Hm). Magnified view shows RGs with endfeet (arrow) or dividing somata (arrowhead) at the ventricle wall (dashed lines). **h**, Fate mapping of E12.5 RGs in *Lhx2-CreER;Ai14* mice reveal PyN progeny across all cortical layers. **i**, Same experiment as in **e** except done at E13.5. *Lhx2*$^{+}$ RGs remain distributed in a medial^{high}-lateral^{low} gradient along the dorsal pallium but at a reduced density compared to earlier stages. Note PyN clones generated from individual RGs (asterisk). **j**, Fate mapping E14.5 RGs in *Lhx2-CreER;Ai14* mice show PyNs across layers, with lower density in L5/6, higher density in L2-4, and highest density in L4. **k**, 24-hour pulse-chase in a E10.5 *Fezf2-CreER;Ai14* embryo. The spatial extent of *Fezf2*$^{+}$ RGs in the dorsal neuroepithelium is much restricted compared to *Lhx2*$^{+}$ RGs at this stage. Magnified view shows RG endfoot (arrow) at the lateral ventricle (dashed lines). Note the sparsity of dividing RGs. **l**, Fate mapping E10.5 RGs using a *Fezf2-CreER;RGBow* mouse. PyN progeny are present in all cortical layers. **m**, Same experiment as in **k** except done at E12.5. *Fezf2*$^{+}$ RGs also distribute in a medial^{high}-lateral^{low} gradient along the dorsal neuroepithelium, ending at the cortex-hem boundary (Hm). Note that *Fezf2*$^{+}$ RG density is much lower than that in **g**. High-magnification views show RGs at multiple cell cycle stages with endfoot (arrow) and dividing soma (arrowhead) at the lateral ventricle wall (dashed line). **n**, Fate mapping E12.5 RGs using sparse labeling in *Fezf2-CreER;Ai14* mice reveal PyNs across cortical layers. **o**, Same experiment as in **k** except done at E13.5. Only sparse *Fezf2*$^{+}$ RGs remain more in medial pallium at this time, when *Fezf2* expression shifts to postmitotic PyNs (arrowheads). Magnified view shows a remaining RG (arrow) at the lateral ventricle (dashed line). Note the presence of largely post-mitotic neurons (arrowheads). **p**, Fate mapping at E17.5 in *Fezf2-CreER;RGBow* labeled only L5b/L6 PyNs in mature cortex. **q**, E16.5 IPs densely labeled by 12-hour pulse-chase in *Tbr2-CreER;Ai14* mice. Magnified view show IP somata (arrowhead) away from the lateral ventricle (dashed line) lacking radial fibers and endfeet. **r**, Fate mapping E16.5 IPs in *Tbr2-CreER;Ai14* mice labels PyNs in L2-3 cortex at P28. **s**, Intersectional fate mapping of neurogenic IPs at E16.5 in *Tis21-CreER;Tbr2-FlpER;Ai65* mice, as depicted in **d,** labeled L2-3 PyN progeny in P28 cortex. **t**, The presence of *Fezf2*$^{-}$ and *Fezf2*$^{+}$ nRGs at E11.5 is revealed by intersection/subtraction fate mapping with 24-hour pulse-chase in *Tis21-CreER;Fezf2-Flp;IS* mice, schematized in **c**. Magnified view shows RFP-labeled *Tis21*$^{+}$*Fezf2*$^{-}$ RGs and GFP-labeled *Tis21*$^{+}$*Fezf2*$^{+}$ RGs. **u**, Fate mapping E11.5 RGs using *Tis21-CreER;Fezf2-Flp;IS* mice The mixed RFP and GFP clone likely derived from a *Tis21*$^{+}$*Fezf2*$^{-}$ RG, which activated RFP expression in all progeny and GFP expression was then switched on only in *Fezf*$^{+}$ postmitotic deep layer PyNs expressing Flp.

a

Projection Class	Lamina	Driver line
IT	L2	**Tbr2-2A-CreER E17**
	L3	**Tbr2-2A-CreER E16**
	L2/3	*^Cux2-Cre*
	L2/3	*^Cux2-CreER*
	L2/3	*Rasgrf2-2A-dCre*
	L2-4	**Cux1-2A-CreER**
	L2/3/5a	**PlxnD1-2A-CreER**
	L2/3/5a	**PlxnD1-2A-Flp**
	L5a	**Tlx3-Cre*
	L4	*Rorb-ires-Cre*
	L4	**Scnn1a-Tg3-Cre*
	L4	**Nr5a1-Cre*
PT	L5b	**Sim1-Cre*
	L5b	**Fezf2-2A-CreER**
	L5b	**Fezf2-2A-Flp**
	L5b	**Adcyap1-2A-CreER**
	L5b	**Tcerg1l-2A-CreER**
	L5b	***^Sema3E-CreER***
CT	L6	**Ntsr1-Cre*
	L6	**Tbr1-2A-CreER**
	L6	**Tle4-2A-CreER**
	L6	**Foxp2-ires-Cre**

* transgenic line; ^ Cre cassette inserted at ATG;
italics, previously generated; bold, presented in this study

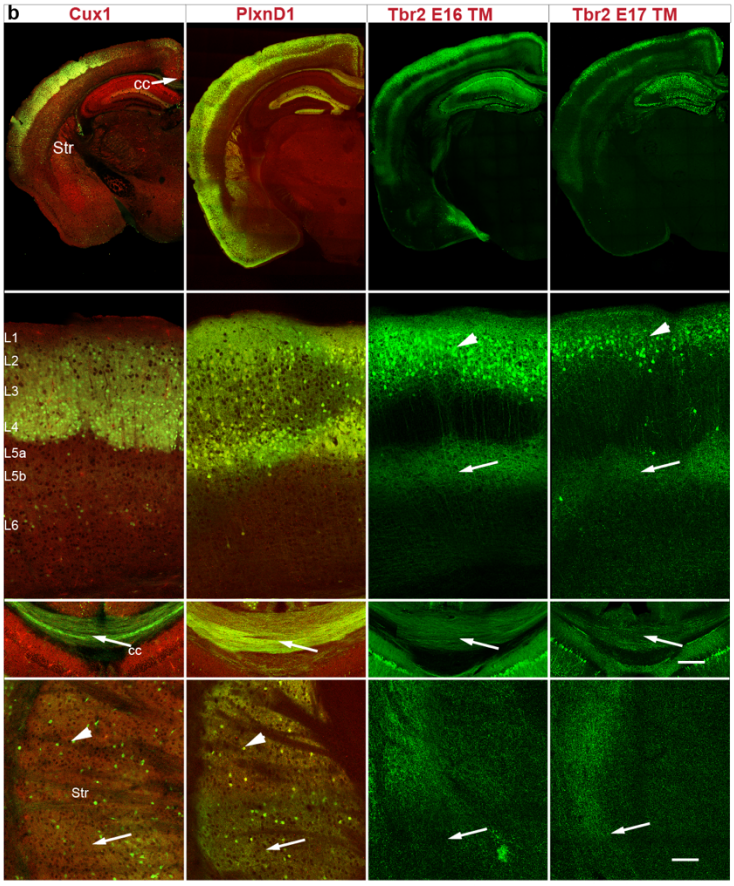

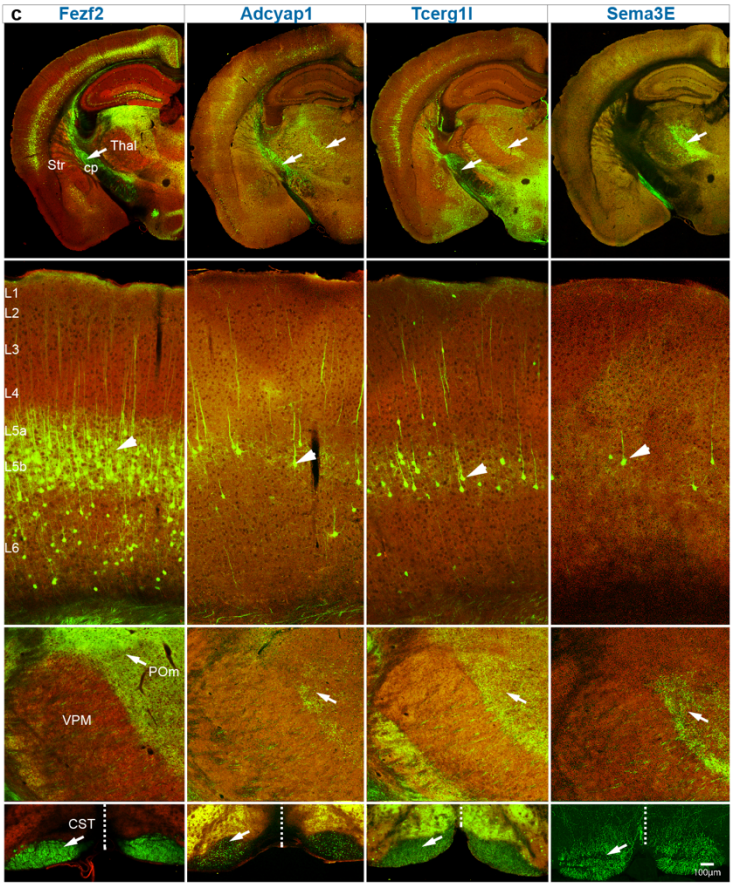

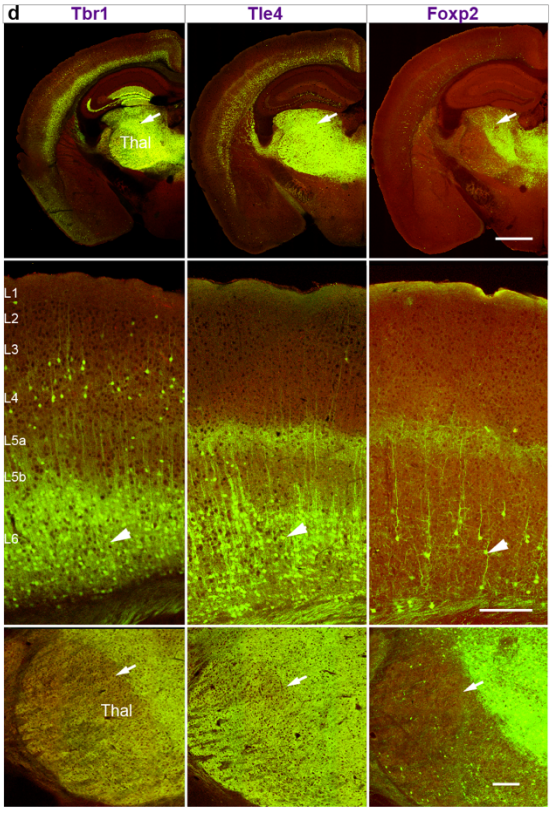

Fig. 3 Genetic targeting of PyN projection classes and subpopulations.
a, List of mouse driver lines generated in this study (bold) in relation to several previously reported and frequently used lines (italic) sorted by projection class and laminar pattern. * indicate transgenic lines. **b-d** show Cre recombination patterns visualized through reporter expression (green) and background autofluorescence (red). Top row: coronal hemisections at Bregma -1.7 mm; second row: a segment of the somatosensory cortex with laminar delineations; third and fourth rows: representative subcortical patterns. **b,** IT drivers label PyNs in L2-4 and L5A, many project across the corpus collusum (cc) and to the striatum (Str). Note *Cux1* and *PlxnD1* drivers also labels subset of medium spiny neurons in the striatum. *Tbr2-CreER* induction at E16 and E17 label L2/3 and L3 PyNs, respectively. Cell bodies are indicated by arrowheads and axons by arrow. **c,** PT drivers label PyNs in L5B, which project to numerous subcortical targets, including the thalamus (thal, third row) and spinal cord (corticospinal tract–CST, fourth row). cp, cerebral peduncle; POm, posterior medial nucleus of thalamus; VPM, ventral posteromedial nucleus of thalamus. **d,** CT drivers label PyNs in L6, with different thalamic nuclei as their major projection targets. TM inductions were at P21 except for *Tbr2-CreER*, as indicated, *Adcyap1-CreER* at E17.5 and *Sema3E-CreER* at P7. The reporter allele was *Ai14*, except for *PlexD1* (*Snap25-LSL-EGFP*) and *Foxp2* (systemic injection of AAV9-CAG-FLEX-EGFP). Scale bars: CST panel in **c**, 100 μm; hemisection in **d** applies to all hemisections, 1mm; all other scalebars, 200 μm.

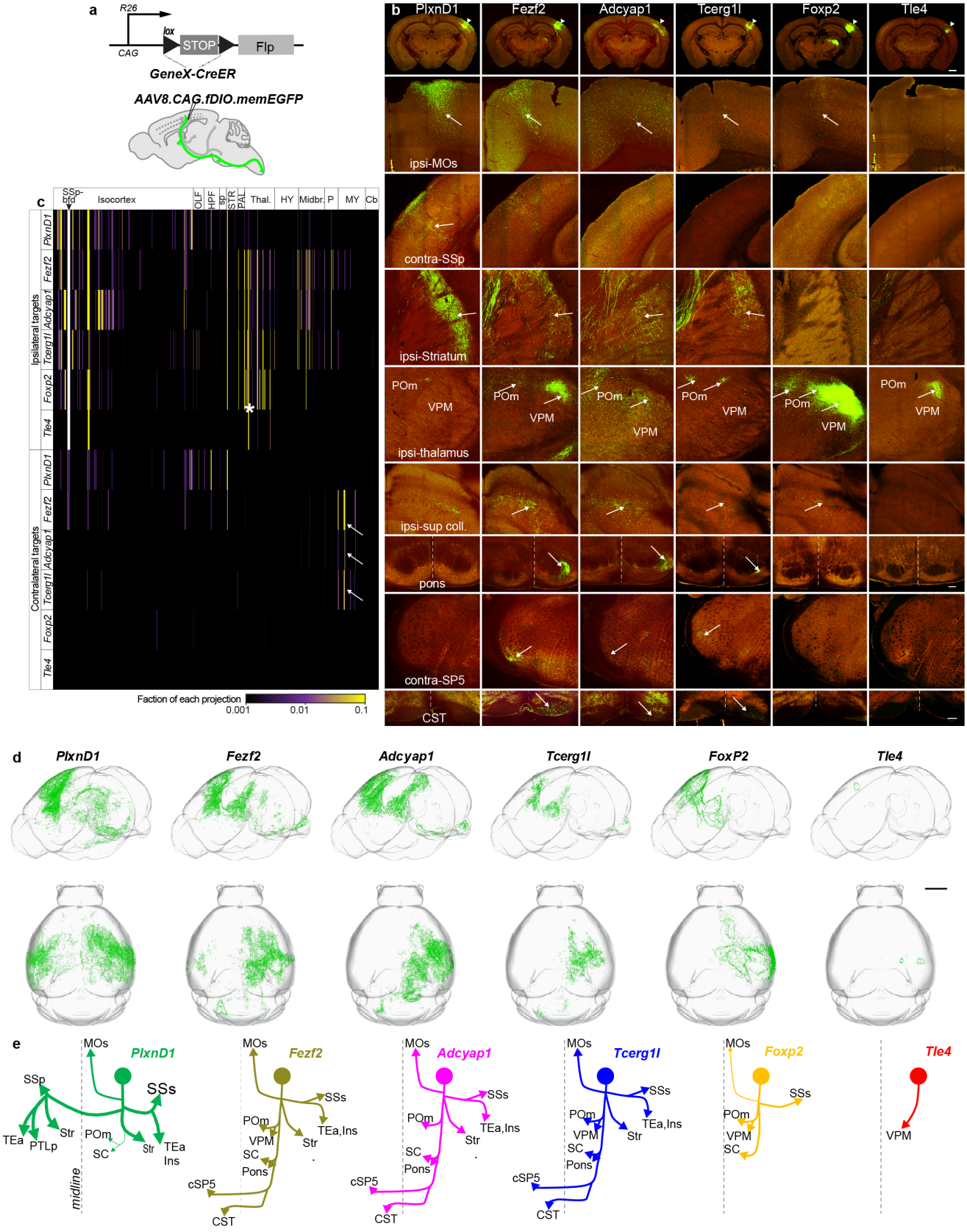

Fig. 4: Anterograde tracing from PyN subpopulations in S1 barrel somatosensory cortex.
a, Strategy for anterograde axon tracing. In a *GeneX-CreER;LSL-Flp* mouse, tamoxifen induction of *CreER* expression at a given time is converted to constitutive *Flp* expression for anterograde tracing with a Flp-dependent AAV vector. **b**, STP images at the S1 injection site (top row, arrow head) and at selected subcortical projection targets for six driver lines, with EGFP or EYFP expression from cell-type specific viral vector (green) and background autofluorescence (red). **c**, Axon projection matrix from SSp-bfd (indicated with an arrowhead) to 682 ipsilateral and 682 contralateral targets, each grouped under 12 major categories, for each of six mouse lines presented in **b**. Each row represents the fraction of total axon signal measured from a single experiment per brain area. Signal in the injection site was subtracted from the whole brain total to show fraction of projections outside the injected region. PyNs^{PlxnD1} project bilaterally to cortex and striatum; PyNs^{Fezf2}, PyNs^{Adcyap1} and PyNs^{Tcerg1l} project to multiple ipsilateral targets and to the contralateral brainstem (arrows); and PyNs^{Foxp2} and PyNs^{Tle4} project to the ipsilateral thalamus (asterisk). **d**, Whole-brain three dimensional renderings of axon projections registered to the CCFv3 for each PyN subpopulation in the S1 cortex with parasagittal view (top) and dorsal view (bottom). **e**, Schematics of main projection targets for each PyN subpopulation. Scale bars: top row in **b**, 1mm; pons panel, 200µm; CST panel (bottom row) in **b** applies to all other panels, 200µm; **d**, 2 mm.

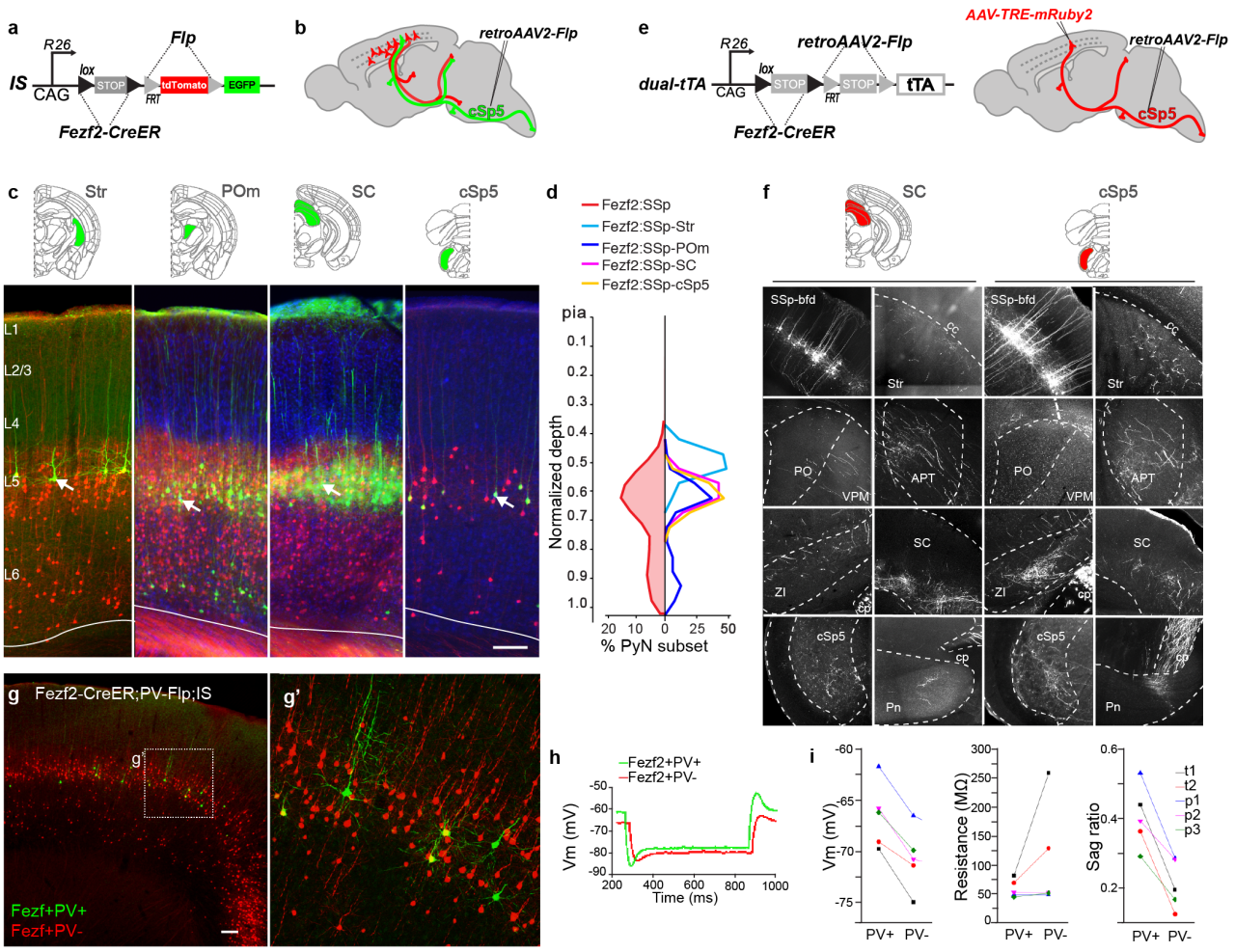

Fig. 5: Intersectional dissection of *Fezf2* subpopulations. a, Intersection-subtraction (IS) strategy to define PyN subpopulations by combinatorial Cre and Flp drivers. **b**, Intersectional strategy to reveal Fezf2 subpopulations by projection target using retrograde retroAAV2-Flp and IS reporter. **c**, Fezf2 somata with a defined projection target (GFP-labeled) show more restricted laminar position in L5 compared to the broad RFP$^+$ Fezf2 PyNs in S1 cortex.**d,** Normalized cortical depth distributions of overall Fezf2 somata (leftward curve) and of each target-defined Fezf2 subpopulation (rightward curves). **e**, Strategy for combinatorial targeting by marker, axon target and soma location ('triple trigger'). The *dual-tTA* reporter expresses the transcription activator tTA upon *Cre* and *Flp* recombination. In a *Fezf2-CreER;dual-tTA* mouse, TM induction combined with retroAAV2-Flp injection at the contralateral spinal trigeminal nucleus (cSp5) activate tTA expression in cSp5-projection PyNs^{Fezf2} across cortical areas, and AAV-TRE-mRuby injection at SSp-bfd then labels cSp5-projection PyNs^{Fezf2} in the SSp-bfd. **f**, Coronal images of PyNs^{Fezf2} in SSp-bfd with projection to SC or cSp5, displaying axon collaterals at various subcortical targets, including Str, ZI, thalamus, pons. **g,** Using the *Fezf2-CreER;Pv-Flp;IS* triple allele mice, PV$^-$ and PV$^+$ PyNs^{Fezf2} can be distinguished by their expression of RFP and GFP, respectively. Boxed area is magnified in **g'**. **h,** Sample voltage responses induced by current injection from a pair of PV$^+$ (green) and PV$^-$ (red) PyNs^{Fezf2} by whole-cell patch recording in a cortical slice. **i,** Electrophysiological differences between 5 pairs of PV$^+$ and PV$^-$ PyNs^{Fezf2}: resting membrane potential (Vm, -66.5 ± 1.6 vs. -70.7 ± 1.5 mV, mean ± s.e.m.; p = 0.0014, Student's paired t-test); input resistance (MΩ, 60.1 ± 7.8 vs. 108.7 ± 45.4 MΩ, mean ± s.e.m.; p = 0.23, Student's paired t-test); Sag ratio (=hyperpolarization (Peak-Steady)/Steady, 0.40 ± 0.05 vs. 0.21 ± 0.04, mean ± s.e.m.; p = 0.0039, Student's paired t-test). Abbreviations: cc, corpus callosum; SSp-bfd, somatosensory barrel field cortex; APT, anteropretectal nucleus; Str, striatum; SC, Superior Colliculus; PO, posterior nucleus of the thalamus; VPM, ventral posteromedial nucleus of the thalamus; cSp5, contralateral spinal trigeminal nucleus; PV, Parvalbumin. Scale bars: **b**, 100µm; **d**, 1 mm; **g**, 100µm.

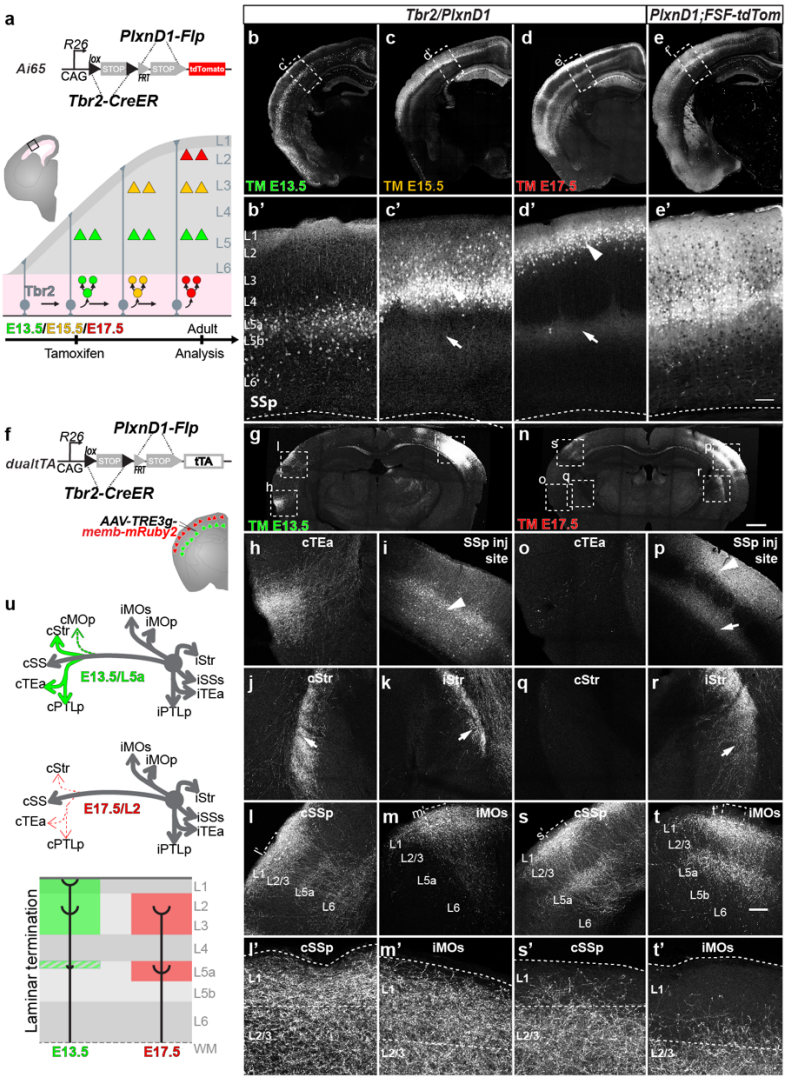

Fig. 6: Combinatorial targeting of PyN subtypes defined by lineage, birth time, anatomical location, projection pattern. a, Strategy for combinatorial labeling of PyNs^{PlxnD1} laminar subsets. In a *Tbr2-CreER;PlxnD1-Flp;Ai65* mouse, tamoxifen (TM) inductions at successive embryonic times label PyNs^{PlexD1} born from intermediate progenitors at these times that occupy deeper and more superficial layers. **b-d,** Representative images of laminar subsets of PyNs^{PlxnD1} born at E13.5 (**b**), E15.5 (**c**), and E17.5 (**d**). **e,** As a comparison, the whole PyNs^{PlxnD1} population is labeled in a *PlxnD1-Flp;R26-CAG-FSF-tdTom* mouse. **b'-e'**, High magnification of boxed regions in **b-d.** Arrowheads indicate cell body positions; arrows indicate axons. **f**, In a *Tbr2-CreER;PlxnD1-Flp;dual-tTA* mouse, TM inductions at E13.5 and E17.5 activates tTA expression in L5A and L2 PyNs^{PlexD1}, respectively; AAV-TRE3g-memb-mRuby2 injection in barrel cortex then reveals the axon projection pattern of each set of laminar specific PyNs^{PlxnD1}. **g-m,** Anterograde tracing from E13.5-born L5A PyNs^{PlxnD1} in SSp-bfd. **g**, Coronal section shows AAV-TRE3g-memb-mRuby2 injection site and several major projection targets. **h-m**, Example images of axon projection targets of several indicated ipsi- and contra-lateral sites. Arrowheads indicate somata; arrows indicate axons. **(n-t)** Anterograde tracing from E17.5-born L2 PyNs^{PlxnD1} in SSp-bfd. **n**, Coronal section shows AAV injection site and several major projection targets. **o-s**, Example images of axon projection targets of several indicated ipsi- and contra-lateral sites. **l',m',s',t'**, Higher magnification of cSSp (**l'** & **s'**) and iMOs (**m'** & **t'**) display laminar axon termination differences between L5A versus L2 PyNs^{PlexD1}, respectively. **u**, Schematic comparison of the projection patterns of E13.5-born L5A versus E17.5-born L2 PyNs^{PlexD1}. L5A and L2 PyNs^{PlexD1} show major differences in strength of several contralateral targets and in the laminar axon termination pattern. Scale bar in: f (refers to c-f), 200 µm; n (refers to g & n), 1 mm; t (refers to h-t), 50µm.

References

1 Harris, K. D. & Shepherd, G. M. The neocortical circuit: themes and variations. *Nat Neurosci* **18**, 170-181, doi:10.1038/nn.3917 (2015).

2 Huang, Z. J. Toward a genetic dissection of cortical circuits in the mouse. *Neuron* **83**, 1284-1302, doi:10.1016/j.neuron.2014.08.041 (2014).

3 Lodato, S. & Arlotta, P. Generating neuronal diversity in the mammalian cerebral cortex. *Annu Rev Cell Dev Biol* **31**, 699-720, doi:10.1146/annurev-cellbio-100814-125353 (2015).

4 Gerfen, C. R., Economo, M. N. & Chandrashekar, J. Long distance projections of cortical pyramidal neurons. *J Neurosci Res* **96**, 1467-1475, doi:10.1002/jnr.23978 (2018).

5 Kawaguchi, Y. Pyramidal Cell Subtypes and Their Synaptic Connections in Layer 5 of Rat Frontal Cortex. *Cereb Cortex* **27**, 5755-5771, doi:10.1093/cercor/bhx252 (2017).

6 Tasic, B. *et al.* Shared and distinct transcriptomic cell types across neocortical areas. *Nature* **563**, 72-78, doi:10.1038/s41586-018-0654-5 (2018).

7 Rakic, P. The radial edifice of cortical architecture: from neuronal silhouettes to genetic engineering. *Brain Res Rev* **55**, 204-219, doi:S0165-0173(07)00035-5 [pii] 10.1016/j.brainresrev.2007.02.010 (2007).

8 Kriegstein, A., Noctor, S. & Martinez-Cerdeno, V. Patterns of neural stem and progenitor cell division may underlie evolutionary cortical expansion. *Nat Rev Neurosci* **7**, 883-890, doi:nrn2008 [pii]10.1038/nrn2008 (2006).

9 Telley, L. *et al.* Temporal patterning of apical progenitors and their daughter neurons in the developing neocortex. *Science* **364**, doi:10.1126/science.aav2522 (2019).

10 Greig, L. C., Woodworth, M. B., Galazo, M. J., Padmanabhan, H. & Macklis, J. D. Molecular logic of neocortical projection neuron specification, development and diversity. *Nat Rev Neurosci* **14**, 755-769, doi:10.1038/nrn3586 (2013).

11 Franco, S. J. *et al.* Fate-restricted neural progenitors in the mammalian cerebral cortex. *Science* **337**, 746-749, doi:337/6095/746 [pii]10.1126/science.1223616.

12 Gil-Sanz, C. *et al.* Lineage Tracing Using Cux2-Cre and Cux2-CreERT2 Mice. *Neuron* **86**, 1091-1099, doi:10.1016/j.neuron.2015.04.019 (2015).

13 Guo, C. *et al.* Fezf2 expression identifies a multipotent progenitor for neocortical projection neurons, astrocytes, and oligodendrocytes. *Neuron* **80**, 1167-1174, doi:10.1016/j.neuron.2013.09.037 (2013).

14 Eckler, M. J. *et al.* Cux2-positive radial glial cells generate diverse subtypes of neocortical projection neurons and macroglia. *Neuron* **86**, 1100-1108, doi:10.1016/j.neuron.2015.04.020 (2015).

15 Gerfen, C. R., Paletzki, R. & Heintz, N. GENSAT BAC cre-recombinase driver lines to study the functional organization of cerebral cortical and basal ganglia circuits. *Neuron* **80**, 1368-1383, doi:10.1016/j.neuron.2013.10.016 (2013).

16 Harris, J. A. *et al.* Anatomical characterization of Cre driver mice for neural circuit mapping and manipulation. *Front Neural Circuits* **8**, 76, doi:10.3389/fncir.2014.00076 (2014).

17 Chou, S. J. & Tole, S. Lhx2, an evolutionarily conserved, multifunctional regulator of forebrain development. *Brain Res* **1705**, 1-14, doi:10.1016/j.brainres.2018.02.046 (2019).

18 Woodworth, M. B., Greig, L. C., Kriegstein, A. R. & Macklis, J. D. SnapShot: cortical development. *Cell* **151**, 918-918 e911, doi:10.1016/j.cell.2012.10.004 (2012).

19 Bulchand, S., Grove, E. A., Porter, F. D. & Tole, S. LIM-homeodomain gene Lhx2 regulates the formation of the cortical hem. *Mech Dev* **100**, 165-175, doi:10.1016/s0925-4773(00)00515-3 (2001).

20 Mangale, V. S. *et al.* Lhx2 selector activity specifies cortical identity and suppresses hippocampal organizer fate. *Science* **319**, 304-309, doi:10.1126/science.1151695 (2008).

21 Monuki, E. S., Porter, F. D. & Walsh, C. A. Patterning of the dorsal telencephalon and cerebral cortex by a roof plate-Lhx2 pathway. *Neuron* **32**, 591-604, doi:10.1016/s0896-6273(01)00504-9 (2001).
22 Shetty, A. S. *et al.* Lhx2 regulates a cortex-specific mechanism for barrel formation. *Proc Natl Acad Sci U S A* **110**, E4913-4921, doi:10.1073/pnas.1311158110 (2013).
23 Chen, B., Schaevitz, L. R. & McConnell, S. K. Fezl regulates the differentiation and axon targeting of layer 5 subcortical projection neurons in cerebral cortex. *Proc Natl Acad Sci U S A* **102**, 17184-17189, doi:10.1073/pnas.0508732102 (2005).
24 Molyneaux, B. J., Arlotta, P., Hirata, T., Hibi, M. & Macklis, J. D. Fezl is required for the birth and specification of corticospinal motor neurons. *Neuron* **47**, 817-831, doi:S0896-6273(05)00732-4 [pii]10.1016/j.neuron.2005.08.030 (2005).
25 Muralidharan, B. *et al.* LHX2 Interacts with the NuRD Complex and Regulates Cortical Neuron Subtype Determinants Fezf2 and Sox11. *J Neurosci* **37**, 194-203, doi:10.1523/JNEUROSCI.2836-16.2016 (2017).
26 Chou, S. J., Perez-Garcia, C. G., Kroll, T. T. & O'Leary, D. D. Lhx2 specifies regional fate in Emx1 lineage of telencephalic progenitors generating cerebral cortex. *Nat Neurosci* **12**, 1381-1389, doi:10.1038/nn.2427 (2009).
27 Godbole, G. *et al.* Hierarchical genetic interactions between FOXG1 and LHX2 regulate the formation of the cortical hem in the developing telencephalon. *Development* **145**, doi:10.1242/dev.154583 (2018).
28 He, M. *et al.* Strategies and Tools for Combinatorial Targeting of GABAergic Neurons in Mouse Cerebral Cortex. *Neuron* **91**, 1228-1243, doi:10.1016/j.neuron.2016.08.021 (2016).
29 Florio, M. & Huttner, W. B. Neural progenitors, neurogenesis and the evolution of the neocortex. *Development* **141**, 2182-2194, doi:10.1242/dev.090571 (2014).
30 Haubensak, W., Attardo, A., Denk, W. & Huttner, W. B. Neurons arise in the basal neuroepithelium of the early mammalian telencephalon: a major site of neurogenesis. *Proc Natl Acad Sci U S A* **101**, 3196-3201, doi:10.1073/pnas.0308600100 (2004).
31 Martinez-Cerdeno, V. *et al.* Evolutionary origin of Tbr2-expressing precursor cells and the subventricular zone in the developing cortex. *J Comp Neurol* **524**, 433-447, doi:10.1002/cne.23879 (2016).
32 Martinez-Cerdeno, V., Noctor, S. C. & Kriegstein, A. R. The role of intermediate progenitor cells in the evolutionary expansion of the cerebral cortex. *Cereb Cortex* **16 Suppl 1**, i152-161, doi:10.1093/cercor/bhk017 (2006).
33 Sun, T. & Hevner, R. F. Growth and folding of the mammalian cerebral cortex: from molecules to malformations. *Nat Rev Neurosci* **15**, 217-232, doi:10.1038/nrn3707 (2014).
34 Kowalczyk, T. *et al.* Intermediate neuronal progenitors (basal progenitors) produce pyramidal-projection neurons for all layers of cerebral cortex. *Cereb Cortex* **19**, 2439-2450, doi:10.1093/cercor/bhn260 (2009).
35 Mihalas, A. B. *et al.* Intermediate Progenitor Cohorts Differentially Generate Cortical Layers and Require Tbr2 for Timely Acquisition of Neuronal Subtype Identity. *Cell Rep* **16**, 92-105, doi:10.1016/j.celrep.2016.05.072 (2016).
36 Vasistha, N. A. *et al.* Cortical and Clonal Contribution of Tbr2 Expressing Progenitors in the Developing Mouse Brain. *Cereb Cortex* **25**, 3290-3302, doi:10.1093/cercor/bhu125 (2015).
37 Englund, C. *et al.* Pax6, Tbr2, and Tbr1 are expressed sequentially by radial glia, intermediate progenitor cells, and postmitotic neurons in developing neocortex. *J Neurosci* **25**, 247-251, doi:10.1523/JNEUROSCI.2899-04.2005 (2005).
38 Kawaguchi, A. *et al.* Single-cell gene profiling defines differential progenitor subclasses in mammalian neurogenesis. *Development* **135**, 3113-3124, doi:10.1242/dev.022616 (2008).

39 Noctor, S. C., Martinez-Cerdeno, V., Ivic, L. & Kriegstein, A. R. Cortical neurons arise in symmetric and asymmetric division zones and migrate through specific phases. *Nature neuroscience* **7**, 136-144, doi:10.1038/nn1172nn1172 [pii] (2004).

40 Arlotta, P., Molyneaux, B. J., Jabaudon, D., Yoshida, Y. & Macklis, J. D. Ctip2 controls the differentiation of medium spiny neurons and the establishment of the cellular architecture of the striatum. *J Neurosci* **28**, 622-632, doi:28/3/622 [pii]10.1523/JNEUROSCI.2986-07.2008 (2008).

41 Fame, R. M., MacDonald, J. L. & Macklis, J. D. Development, specification, and diversity of callosal projection neurons. *Trends Neurosci* **34**, 41-50, doi:S0166-2236(10)00147-5 [pii]10.1016/j.tins.2010.10.002 (2011).

42 Arlotta, P. *et al.* Neuronal subtype-specific genes that control corticospinal motor neuron development in vivo. *Neuron* **45**, 207-221, doi:10.1016/j.neuron.2004.12.036 (2005).

43 Hintiryan, H. *et al.* The mouse cortico-striatal projectome. *Nat Neurosci* **19**, 1100-1114, doi:10.1038/nn.4332 (2016).

44 Zingg, B. *et al.* Neural networks of the mouse neocortex. *Cell* **156**, 1096-1111, doi:10.1016/j.cell.2014.02.023 (2014).

45 Hooks, B. M. *et al.* Topographic precision in sensory and motor corticostriatal projections varies across cell type and cortical area. *Nat Commun* **9**, 3549, doi:10.1038/s41467-018-05780-7 (2018).

46 Nieto, M. *et al.* Expression of Cux-1 and Cux-2 in the subventricular zone and upper layers II-IV of the cerebral cortex. *J Comp Neurol* **479**, 168-180, doi:10.1002/cne.20322 (2004).

47 Weiss, L. A. & Nieto, M. The crux of Cux genes in neuronal function and plasticity. *Brain Res* **1705**, 32-42, doi:10.1016/j.brainres.2018.02.044 (2019).

48 Cubelos, B. *et al.* Cux-2 controls the proliferation of neuronal intermediate precursors of the cortical subventricular zone. *Cereb Cortex* **18**, 1758-1770, doi:10.1093/cercor/bhm199 (2008).

49 Cubelos, B. *et al.* Cux1 and Cux2 regulate dendritic branching, spine morphology, and synapses of the upper layer neurons of the cortex. *Neuron* **66**, 523-535, doi:10.1016/j.neuron.2010.04.038 (2010).

50 Rodriguez-Tornos, F. M. *et al.* Cux1 Enables Interhemispheric Connections of Layer II/III Neurons by Regulating Kv1-Dependent Firing. *Neuron* **89**, 494-506, doi:10.1016/j.neuron.2015.12.020 (2016).

51 Ding, J. B., Oh, W. J., Sabatini, B. L. & Gu, C. Semaphorin 3E-Plexin-D1 signaling controls pathway-specific synapse formation in the striatum. *Nat Neurosci* **15**, 215-223, doi:10.1038/nn.3003 (2011).

52 Oh, W. J. & Gu, C. The role and mechanism-of-action of Sema3E and Plexin-D1 in vascular and neural development. *Semin Cell Dev Biol* **24**, 156-162, doi:10.1016/j.semcdb.2012.12.001 (2013).

53 Molyneaux, B. J. *et al.* Novel subtype-specific genes identify distinct subpopulations of callosal projection neurons. *J Neurosci* **29**, 12343-12354, doi:29/39/12343 [pii]10.1523/JNEUROSCI.6108-08.2009 (2009).

54 Leone, D. P., Srinivasan, K., Chen, B., Alcamo, E. & McConnell, S. K. The determination of projection neuron identity in the developing cerebral cortex. *Curr Opin Neurobiol* **18**, 28-35, doi:10.1016/j.conb.2008.05.006 (2008).

55 Lodato, S. *et al.* Gene co-regulation by Fezf2 selects neurotransmitter identity and connectivity of corticospinal neurons. *Nat Neurosci* **17**, 1046-1054, doi:10.1038/nn.3757 (2014).

56 Chauvet, S. *et al.* Gating of Sema3E/PlexinD1 signaling by neuropilin-1 switches axonal repulsion to attraction during brain development. *Neuron* **56**, 807-822, doi:10.1016/j.neuron.2007.10.019 (2007).

57 Watakabe, A., Ohsawa, S., Hashikawa, T. & Yamamori, T. Binding and complementary expression patterns of semaphorin 3E and plexin D1 in the mature neocortices of mice and monkeys. *J Comp Neurol* **499**, 258-273, doi:10.1002/cne.21106 (2006).

58 Pecho-Vrieseling, E., Sigrist, M., Yoshida, Y., Jessell, T. M. & Arber, S. Specificity of sensory-motor connections encoded by Sema3e-Plxnd1 recognition. *Nature* **459**, 842-846, doi:10.1038/nature08000 (2009).

59 Mihalas, A. B. & Hevner, R. F. Control of Neuronal Development by T-Box Genes in the Brain. *Curr Top Dev Biol* **122**, 279-312, doi:10.1016/bs.ctdb.2016.08.001 (2017).

60 Han, W. *et al.* TBR1 directly represses Fezf2 to control the laminar origin and development of the corticospinal tract. *Proc Natl Acad Sci U S A* **108**, 3041-3046, doi:10.1073/pnas.1016723108 (2011).

61 Molyneaux, B. J. *et al.* DeCoN: genome-wide analysis of in vivo transcriptional dynamics during pyramidal neuron fate selection in neocortex. *Neuron* **85**, 275-288, doi:10.1016/j.neuron.2014.12.024 (2015).

62 Kast, R. J., Lanjewar, A. L., Smith, C. D. & Levitt, P. FOXP2 exhibits projection neuron class specific expression, but is not required for multiple aspects of cortical histogenesis. *Elife* **8**, doi:10.7554/eLife.42012 (2019).

63 Chang, M., Suzuki, N. & Kawai, H. D. Laminar specific gene expression reveals differences in postnatal laminar maturation in mouse auditory, visual, and somatosensory cortex. *J Comp Neurol* **526**, 2257-2284, doi:10.1002/cne.24481 (2018).

64 Rousso, D. L. *et al.* Two Pairs of ON and OFF Retinal Ganglion Cells Are Defined by Intersectional Patterns of Transcription Factor Expression. *Cell Rep* **15**, 1930-1944, doi:10.1016/j.celrep.2016.04.069 (2016).

65 Daigle, T. L. *et al.* A Suite of Transgenic Driver and Reporter Mouse Lines with Enhanced Brain-Cell-Type Targeting and Functionality. *Cell* **174**, 465-480 e422, doi:10.1016/j.cell.2018.06.035 (2018).

66 Laboulaye, M. A., Duan, X., Qiao, M., Whitney, I. E. & Sanes, J. R. Mapping Transgene Insertion Sites Reveals Complex Interactions Between Mouse Transgenes and Neighboring Endogenous Genes. *Front Mol Neurosci* **11**, 385, doi:10.3389/fnmol.2018.00385 (2018).

67 Winnubst, J. *et al.* Reconstruction of 1,000 Projection Neurons Reveals New Cell Types and Organization of Long-Range Connectivity in the Mouse Brain. *Cell* **179**, 268-281 e213, doi:10.1016/j.cell.2019.07.042 (2019).

68 Wang, X. *et al.* Genetic Single Neuron Anatomy Reveals Fine Granularity of Cortical Axo-Axonic Cells. *Cell Rep* **26**, 3145-3159 e3145, doi:10.1016/j.celrep.2019.02.040 (2019).

69 Arlotta, P. & Hobert, O. Homeotic Transformations of Neuronal Cell Identities. *Trends Neurosci* **38**, 751-762, doi:10.1016/j.tins.2015.10.005 (2015).

70 Hodge, R. D. *et al.* Conserved cell types with divergent features in human versus mouse cortex. *Nature* **573**, 61-68, doi:10.1038/s41586-019-1506-7 (2019).

71 Doan, R. N. *et al.* Mutations in Human Accelerated Regions Disrupt Cognition and Social Behavior. *Cell* **167**, 341-354 e312, doi:10.1016/j.cell.2016.08.071 (2016).

72 Blankvoort, S., Witter, M. P., Noonan, J., Cotney, J. & Kentros, C. Marked Diversity of Unique Cortical Enhancers Enables Neuron-Specific Tools by Enhancer-Driven Gene Expression. *Curr Biol* **28**, 2103-2114 e2105, doi:10.1016/j.cub.2018.05.015 (2018).